X-ray Scattering From Liquid Surfaces: Effect of Resolution†

P. S. Pershan*

SEAS and Department of Physics, Harvard University, Cambridge, Massachusetts 02138

Received: July 10, 2008; Revised Manuscript Received: September 15, 2008

Quantitative interpretation of X-ray reflectivity measurements from liquid surfaces requires methodical accounting of the effects of diffuse scattering from thermal capillary roughness. In this paper we discuss how this requires careful attention to the shape of the experimental resolution. These considerations, which are essential for measurement of the intrinsic structure factor of a liquid surface, require knowledge of the liquid surface tension. The paper closes with a brief comment on the most sensitive method for extraction of the surface tension from measurement of the off-specular diffuse scattering.

1. Introduction

During Pierre G's last visit to Harvard in Oct. of 2006, we discussed much of the material of this article. As always, his thoughts, even on subjects that were not themselves central to his own research, proved to be of valuable assistance to my own ideas, and I am happy to have the opportunity to contribute to the memorial of a fine man, an exemplary scholar, and a much-appreciated teacher.

An enlightening synopsis of X-ray reflectivity was presented by Daillant and Gibaud.[1] They observed that it was slightly more than a century ago that Röntgen answered the question, "Can X-rays be reflected like light"? with the remark that "no noticeable regular reflection of the rays (X-ray) takes place from any of the substances examined".[2] In that time when scientific progress moved at a much slower pace than now, it took nearly three decades before Compton drew attention to the theoretical fact that X-ray reflectivity from most materials is to be expected.[3] It then took a few more years before experiments confirmed Compton's ideas.[4−9] It is unfortunate that as a result of two practical issues X-ray reflectivity remained relatively dormant for the better part of the 20th century.

2. X-Ray Reflectivity

The first of these issues has to do with the relatively weak interaction between X-rays and electrons. To a very good approximation this can be parametrized by what is known as the critical wavevector[1,10]

$$q_c = 4\sqrt{\pi\rho_\infty r_0} \tag{1}$$

where ρ_∞ is the electron density in the bulk, and r_0 is the classical radius of the electron. For a material such as water, $q_c \approx 0.021$ Å^{-1}. This can be compared to the scattering wavevector for an X-ray of wavelength λ that is incident on the surface at an angle α.

$$q_z(\alpha) = (4\pi/\lambda)\sin\alpha \tag{2}$$

For a wavelength $\lambda \approx 1$ Å, the critical angle at which $q_z(\alpha_c) \approx q_c$ is on the order of $\alpha_c \approx 0.1°$. When $\alpha \leq \alpha_c$, the reflectivity from a flat surface is nearly 100%; however, even for an ideal flat surface (zero roughness) the predicted reflectivity falls rapidly with increasing angle, and for $\alpha \geq 5\alpha_c$, the Fresnel reflectivity for the ideal vacuum/material interface[1,10]

$$R_F(q_z) \approx |(q_z - \sqrt{q_z^2 - q_c^2})/(q_z + \sqrt{q_z^2 - q_c^2})|^2 \approx (q_c/2q_z)^4 \tag{3}$$

has fallen by more than 5 orders of magnitude when $\alpha \approx 1°$. When this is combined with the relative weakness of the X-ray sources that were available to early researchers, one can appreciate why for most of the 20th century the scope of possible X-ray reflectivity measurements was severely limited. The breakthrough paper in which Parratt developed a mathematical procedure by which the angular, α or $q_z(\alpha)$, dependence of the reflectivity can be related to the electron density profile along the surface normal illustrates what was possible at that time.[11] Unfortunately, as can be seen from Parratt's paper, the relevant measurements were limited to small values of q_z and, correspondingly, the resolution by which the profile was determined was not much better than tens of angstroms.

Things were improved somewhat following the development of the higher brilliance rotating anode X-ray sources that became available in the 1970s; however, the major breakthroughs were only achieved in the mid 1980s with the availability of even higher brilliance synchrotron X-ray sources.[1,12] The principal goal of nearly all of the X-ray reflectivity studies is to determine the average electron density profile along the surface normal

$$\langle\rho(z)\rangle \approx A_{xy}^{-1}\int_{A_{xy}} d^2\vec{r}_{xy}\rho(\vec{r}_{xy}, z) \tag{4}$$

where A_{xy} is some empirically defined surface area. For solid surfaces, $\langle\rho(z)\rangle$ becomes independent of A_{xy} as soon $\sqrt{A_{xy}}$ becomes larger than a few times the atomic size. The different situation for liquid surfaces will be discussed below. Nevertheless, for solid surfaces and for some cases of liquids, the surface profile can be related to the measured reflectivity using a Born approximation.[10,13] The most useful result has been termed the *master formula*,

* E-mail: pershan@seas.harvard.edu.

† Part of the "PGG (Pierre-Gilles de Gennes) Memorial Issue".

10.1021/jp806113n CCC: $40.75
Published on Web 11/11/2008

$$R^0(q_z) \approx R_F(q_z)|\Phi^T(q_z)|^2 \quad (5)$$

where the surface structure factor is approximated by

$$\Phi^T(q_z) = \rho_\infty^{-1} \int dz[d\langle\rho(z)\rangle/dz]\exp[iq_z z] \quad (6)$$

Strictly speaking, the combination of eqs 5 and 6 is only valid for $q_z \geq 4$ or $5q_c$; however, unless the width of the surface transion region over which $\langle\rho(z))\rangle$ grows from zero to $\sim\rho_\infty$ is much greater than $2\pi/q_c$, these equations are quite accurate.[1,12] Otherwise, the method developed by Parratt can be used to relate $R^0(q_z)$ to $\langle\rho(z)\rangle$.[11]

The primary effect that limits the minimum length scale for which features of $\langle\rho(z)\rangle$ can be determined is the maximum value of q_z for which $R^0(q_z)$can be measured. Although one obvious limit occurs when $R^0(q_z)$ falls to a level that the signal-to-noise is immeasurably small, another practical limit occurs when the specular reflectivity falls too far below the intensity of the off-specular diffuse scattering. For some liquids the limiting diffuse scattering is due to scattering from the bulk material below the surface; however, other sources such as air scattering or scattering from the windows of the chamber containing the liquid can be significant. In this context it is important to recognize that the fall-off with increasing q_z is actually much stronger than that of $R_F(q_z)$. For example, for a surface such as the water/vapor interface, which can be well-approximated as having uniform density below a Gaussian rough interface such as that sketched schematically in Figure 1, the average electron density might have the form of an error function whose derivative is Gaussian

$$d\langle\rho\rangle/dz = \rho_\infty(2\pi\sigma_0^2)^{-1/2}\exp[-z^2/2\sigma_0^2] \quad (7)$$

On taking the Fourier transform, $\Phi^T(q_z) = \exp[-\sigma_0^2 q_z^2/2]$ and

$$R^0(q_z) \approx (q_c/2q_z)^4\exp[-q_z^2\sigma_0^2] \quad (8)$$

As presented here the factor $\exp[-q_z^2\sigma_0^2]$ is essentially a Debye−Waller (DW) factor; however, a similar effect would occur for a flat surface (i.e., zero roughness) if the transition from vapor to bulk liquid had the same gradual increase in electron density as the error function. For practical measurements, σ_0 is never less than 1 or 2 Å; however, it can be very much larger.[1,12] The net effect if, for example, $\sigma_0 \approx 2$ Å, is that well before q_z reaches 2 Å^{-1}, $R^0(q_z)$ will have fallen by approximately 12 orders of magnitude, and this is close to the limit of any but the most brilliant synchrotron X-ray reflectometers.

Although the forms of $d\langle\rho\rangle/dz$ and $R^0(q_z)$ in eqs 7 and 8 are reasonably good approximations to the properties of simple liquids such as water and other relatively small molecules such as molten alkanes[14,15] for liquid crystals, liquid metals and numerous other materials' $d\langle\rho\rangle/dz$ exhibit a number of oscillations that induce a corresponding structure in $\Phi^T(q_z)$.[10,16] The more general expression for the reflectivity of solid surfaces is

$$R(q_z) \approx (q_c/2q_z)^4|\Phi(q_z)|^2\exp[-q_z^2\sigma_0^2] \quad (9)$$

where the effect of surface roughness, $\exp[-q_z^2\sigma_0^2]$ has been explicitly introduced to separate it from the intrinsic structure factor $|\Phi(q_z)|^2$, which arises from the variation in the electron density below the interface.

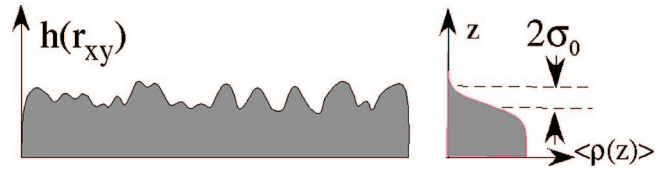

Figure 1. (Left) Schematic illustration of the height fluctuations for a surface section and (right) the electron density profile for an average section.

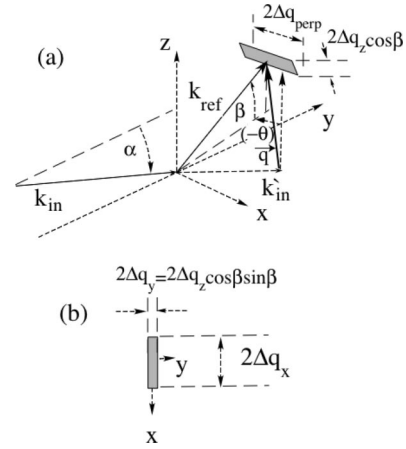

Figure 2. (a) Kinematics of X-ray scattering from a flat surface (i.e., *xy* plane). For specular reflectivity, the Fresnel condition that the reflection angle β is equal to the incident angle α and that the reflection is in the plane of incidence, $\theta = 0$, can be described in terms of the wave vector transfer $\vec{q} = q_z\hat{Z} = (4\pi/\lambda)\sin\hat{\alpha}z$ with $q_x = q_y = 0$. The shaded rectangle illustrates the resolution-determining detector aperture with widths Δq_{perp} transverse to the plane of incidence and $\Delta q_z/\cos\beta$ in the plane. (b) The projection of the resolution onto the *xy* surface is shown for $\theta = 0$. The projection is reduced along the plane of incidence by $\sin\beta$.

In principal, the only way to empirically distinguish whether the q_z dependence of $R(q_z)$ is due to surface roughness or due to gradual nonrough growth of $\langle\rho(z)\rangle$ is to measure diffuse scattering away from the specular condition. Unfortunately, for many measurements there are other sources of diffuse scattering, and the distinction can be ambiguous.

A very fortunate aspect of Fresnel reflectivity is that it is restricted to the condition that the angle that the reflected beam makes with the surface is the same as that of the incident beam and that the scattering is within the plane of incidence. A schematic representation of the kinematics of X-ray reflectivity that is shown in Figure 2 illustrates the fact that this condition for specular reflectivity can also be specified by stipulating that the component of the wavevector transfer parallel $\vec{q}_{xy} = 0$ where

$$\vec{q}_{xy} = (2\pi/\lambda)[\hat{x}\sin\theta + \hat{y}(\cos\alpha - \cos\theta\cos\beta)] = 0 \quad (10)$$

Formally, the differential cross section from a solid surface has the form

$$d\sigma/d^2\vec{q}_{xy} \sim |\Phi(q_z)|^2\delta^2(\vec{q}_{xy})\exp[-\sigma^2 q_z^2] + S(\vec{q}_{xy}) \quad (11)$$

where the delta-function corresponds to the specular reflection. The $S(\vec{q}_{xy})$ describes off-specular diffuse scattering from surface roughness, and the DW factor, $\exp[-\sigma^2 q_z^2]$, accounts for the

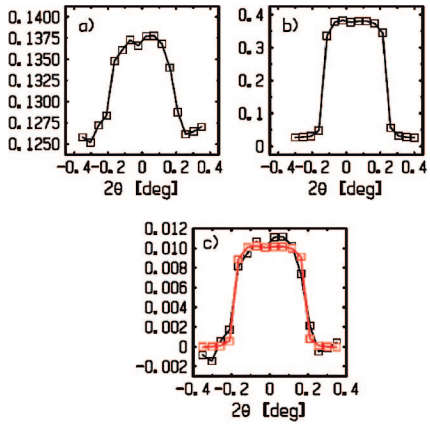

Figure 3. Transverse (i.e., 2θ) scans that illustrate the identification of the specular reflection in the presence of nonspecular diffuse scattering. The units for the vertical scales are arbitrary. The data is from the surface of liquid Bi at $T = 513$ K. The scans in panels a and b were taken at $q_z = 1.6$ and 1.0 Å^{-1}, respectively. The plot in panel c illustrates that when the two scans are scaled the shapes of the specular peaks are identical.[17]

amount by which the reflectivity is reduced due to the roughness-induced diffuse scattering represented by $S(\vec{q}_{xy})$. For practical synchrotron measurements, the X-ray beam incident on the surface is essentially monochromatic and highly collimated. In this situation, for given values of α, β, and θ, the ratio of the measured intensity to the incident intensity is obtained by integrating $d\sigma/d^2\vec{q}_{xy}$over the experimental resolution function. For practical purposes, a very good approximation to the resolution function is is obtained by integration of the solid angle $\Delta\Omega \approx (2\Delta q_x)(2\Delta q_z \cos \beta)/k^2$, which is defined by the detector slit

$$I(\alpha;\beta,\theta)/I_0 = \int_{A_{\text{res}}^{q_{xy}}} d^2\vec{q}_{xy}(d\sigma/d^2\vec{q}_{xy}) \qquad (12)$$

where $A_{\text{res}}^{q_{xy}}$ is the area in $\vec{q}_{xy}$-space of the projection of the detector resolution function on the surface (Figure 2b). If the detector is held at the condition $\beta = \alpha$ while the angle θ is scanned, the specular signal with be a relatively well-defined peak centered at $\theta = 0$ whose shape is essentially determined by the convolution of the detector resolution with the δ-function term in $d\sigma/d^2\vec{q}_{xzy}$. This is a powerful tool by which the specular signal can be determined in the presence of relatively strong nonspecular diffuse scattering. For example, Figure 3 shows data in which the intensity is measured from the surface of liquid Bi as a function of the out-of-plane angle θ.[17] In the next section we will discuss the difference between scattering from liquid and solids surfaces; however, for the moment that difference is not important. The data shown in Figure 3a was recorded at $q_z = 1.6$ Å^{-1}, for which the diffuse scattering from the bulk liquid structure factor is an order of magnitude more intense than the specular signal at $\theta = 0$. The fact that the peak has the shape of the slit-determined resolution function can be seen by comparing it with the equivalent scan in Figure 3b at $q_z = 1.0$ Å^{-1}, for which the bulk diffuse scattering is virtually zero. When the background due to the bulk diffuse scattering is subtracted from the data in Figure 3a and the amplitudes are scaled, as is shown in Figure 3c, the two shapes can be seen to be identical.[18,19] The amplitude of the slit-determined resolution shape in Figure 3a is the specular signal.

X-ray specular reflectivity from solid surfaces have been extensively reviewed[1,10,12] and will not be further discussed in this article other than to reiterate that eq 9 is the result that is obtained from integration of eq 11. On the other hand, the effect of thermal capillary waves on liquid surfaces is to induce the very different surface roughness that causes X-ray reflectivity from liquids to be qualitatively different from that of solids.[20]

3. Effect of Capillary Fluctuations

In contrast to solids, the only two things that keep the surface of bulk liquids flat are gravity and surface tension. Gravity, on the one hand, is a relativity weak force, and its effect is only manifest for surface waves with wavelengths on the order of a gravity-determined scale that is millimeters or longer, that is, $|\vec{q}_{xy}| \leq 10^{-6}$ Å^{-1}. In view of the fact that most X-ray reflectometers can not resolve such long wavelengths (i.e., small q_{xy}), the measured roughness of the liquid surface is dominated by surface tension. The surprising effect is that, in contrast with solid surfaces, for liquids, simple hydrodynamic theory predicts that there is a range of several orders of magnitude, capillary length scale (~1 mm) > r_{xy} > atomic scale (1 nm),[21] for which the height−height correlation function for the liquid grows logarithmically with distance.[22−24]

$$\langle h(\vec{r}_{xy})h(0) - h(0)^2\rangle \approx (kT/2\pi\gamma)\ln(q_{\max}r_{xy}) \qquad (13)$$

The factor $q_{\max} \approx \pi/r_{\text{atom}}$, which is introduced to ensure that $\langle h(\vec{r}_{xy})h(0) - h(0)^2\rangle \rightarrow 0$ as $r_{xy} \rightarrow r_{\text{atom}}$, the atomic radius, is analogous to the phonon wavevector cutoff that is common to the Debye treatment of the solids.[25,26] It follows that, in place of eq 11, the differential cross-section for scattering from the liquid surface has the form[20]

$$\frac{d\sigma}{d^2\vec{q}_{xy}} \approx A_0\left(\frac{q_c}{2q_z}\right)^4 |\Phi(q_z)|^2\left(\frac{q_{xy}}{q_{\max}}\right)^{\eta}\left(\frac{\eta}{2\pi q_{xy}^2}\right) \qquad (14)$$

where

$$\eta = (k_B T/2\pi\gamma)q_z^2 \qquad (15)$$

So long as $\eta < 2$, this form for $A_0^{-1}d\sigma/d^2\vec{q}_{xy}$ has a cusp-shaped peak at $\vec{q}_{xy} = 0$, and although it satisfies a sum rule

$$A_0^{-1}\int_{|q_{xy}|<q_{\max}} d^2\vec{q}_{xy}(d\sigma/d^2\vec{q}_{xy}) = (q_c/2q_z)^4|\Phi(q_z)|^2 \qquad (16)$$

that is similar to one that one might expect for eq 9, it differs from the δ-function form in that, if the integral is limited to a resolution region $|q_{xy}| < q_{\text{res}} < q_{\max}$, the value of the integral depends on the size of the resolution, q_{res}. As a practical matter, the q_{xy} cusp in eq 14 is sufficiently sharp that over the range of the resolution; the variations in q_z with β, or q_y, are small enough that the integral can treated as though $|\Phi(q_z)|$ were constant. Furthermore, for small values of η (i.e., ≪1), the singularity at the cusp is strong enough that the integration over the δ-function and the $1/q_{xy}^2$singularity are close enough that, for all practical purposes, there is no real difference in the measurements of the specular reflectivity from liquid and solid surfaces. On the other hand, as $\eta \rightarrow 1$ the differences become quite significant.

4. Resolution Effect for Liquid Surfaces

The essential point that this paper addresses has to do with the dependence of the measured reflectivity signal

$$I(\alpha;\alpha,0)/I_0 = R(q_z) \approx \int_{A_{\mathrm{res}}^{q_{xy}}} \mathrm{d}^2\vec{q}_{xy}(\mathrm{d}\sigma/\mathrm{d}^2\vec{q}_{xy}) \qquad (17)$$

on the size and shape of $A_{\mathrm{res}}^{q_{xy}}$ when $\eta > 1$. The simplest heuristic way in which the effect can be illustrated is to assume that $A_{\mathrm{res}}^{q_{xy}}$ defines a circle that includes all scattering for which $|\vec{q}_{xy}| < \Delta q_{\mathrm{res}}$. The specular reflectivity predicted by integration using this circular resolution function is

$$R(q_z) \approx (q_c/2q_z)^2|\Phi(q_z)|^2(\Delta q_{\mathrm{res}}/q_{\mathrm{max}})^{\eta} \qquad (18)$$

which can be expressed in the same form as for solids, that is, eq 9, by writing the capillary roughness as

$$\sigma_{\mathrm{cap}}^2 = (k_{\mathrm{B}}T/2\pi\gamma)\ln(q_{\mathrm{max}}/\Delta q_{\mathrm{res}}) \qquad (19)$$

This is the form that was used to interpret the first X-ray scattering experiments from the surface of water and other simple liquids.[14,27,28] Daillant et al. treated the short distance cutoff differently; however, they used the same model for the resolution with equivalent results.[29] The important point illustrated by this result is that the average surface roughness decreases as the diameter of the resolution area increases, approaching zero as $\Delta q_{\mathrm{res}} \rightarrow q_{\mathrm{max}}$.[28] The physics of this is the same as for the DW factor, that is, the decrease in specular reflectivity occurs because capillary waves scatter radiation away from the specular condition; however, if the resolution is sufficiently wide that the detector collects all of the diffuse scattering, then the signal is not reduced. For liquids, this is only relevant for $\eta < 2$. As will be seen below, it is only so long as $\eta < 2$ that the integrated intensity has a maximum at the specular condition, $\vec{q}_{xy} = 0$, which can be interpreted as specular reflectivity. The important issue is to develop a practical empirical procedure for extracting $|\Phi(q_z)|^2$ from the intensity that is measured at the specular condition.

Although the simplicity of eq 18 is compelling, the actual projection of the resolution on to the liquid surface that is illustrated in Figure 2b is rectangular rather than circular. Assuming a rectangular detector slit (height × width = $h \times w$) that is a distance L from the sample, when $\theta = 0$ the projection $A_{\mathrm{res}}^{q_{xy}}$ onto the surface is a rectangle,

$$\begin{aligned} \Delta q_y &= (2\pi/\lambda)(h/L)\sin\beta\cos\beta \\ \Delta q_x &= (2\pi/\lambda)(w/L)\cos\beta \end{aligned} \qquad (20)$$

and it is clear that even if $h \approx w$, for typical reflection angles $\sin\beta \ll 1$, the resolution will generally be strongly asymmetric, $\Delta q_y \ll \Delta q_x$. Braslau et al.[14] may have been the first to evaluate eq 17 by treating $\Delta q_x/\Delta q_y \approx 1/\sin\beta$ for small β as infinite; however, Sinha et al. did the more elegant step by making use of this approximation and integrating eq 17[24] to obtain the 1-dimensional cross section,

$$(\mathrm{d}\sigma^{1\mathrm{D}}/q_y) \approx (q_y^{\eta-1})\int_{-\infty}^{+\infty}\mathrm{d}q_x(\mathrm{d}\sigma/\mathrm{d}^2\vec{q}_{xy}) \qquad (21)$$

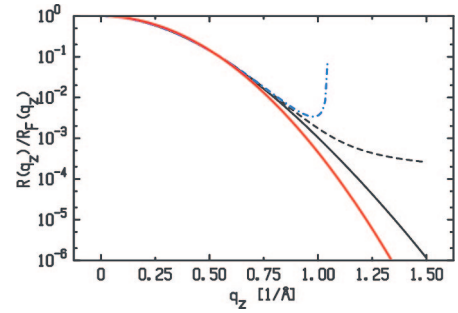

Figure 4. Simulated examples of R/R_{F} for different approximations for the shape of the resolution determining detector slit. (—, black) Projection of the resolution onto the liquid surface is circular. (—•—, blue) Analytic result for the convolution of a Gaussian resolution in the plane of incidence with a slit that is infinitely wide transverse to the plane of incidence. (— — — and —, black) Numerical integrations over slits 300 mm wide and 3 mm wide.

which they then analytically convoluted with a Gaussian resolution function $g(q_y - q_y^0)$. For specular reflectivity $q_y^0 = 0$; however, they also obtained an analytic expression for the near-specular diffuse intensity when $\beta \neq \alpha$, or $q_y^0 \approx (2\pi/\lambda)[\cos\alpha - \cos\beta]$. Assuming that the integral over q_x is some finite constant, the immediate implication of this is that, although for $\mathrm{d}\sigma/\mathrm{d}^2\vec{q}_{xy}$ the peak at $\vec{q}_{xy} = 0$ persists as long as $\eta < 2$, the peak in $(\mathrm{d}\sigma^{1\mathrm{D}}/q_y)$ only persists so long as $\eta < 1$. The implication of this is that for an infinitely wide slit, specular reflectivity can only be defined for a liquid so long as $\eta \leq 1$ or $q_z^2 < (k_{\mathrm{B}}T/2\pi\gamma)^{-1}$. Although this is formally correct, the approximation of an infinitely wide slit is not realistic.

The effect of the infinitely wide resolution on capillary effects is most simply illustrated for a surface such as water in which the structure factor has the form used in eq 8. The broken blue line in Figure 4 (—•—, blue) displays the calculated $R(q_z)/R_{\mathrm{F}}(q_z)$ for water using Sinha's function. The result diverges at the value of q_z, corresponding to $\eta = 1$ ($q_z \approx 1.045$ Å^{-1}). The divergence arises from the fact that $\int_{-\infty}^{+\infty}\mathrm{d}q_x(q_x^2 + q_y^2)^{\eta/2-1}$ is only finite when $\eta < 1$. The solid red line (—) demonstrates that for $q_z \leq 0.7$ the circular resolution and the infinitely wide resolution give essentially the same $R(q_z)/R_{\mathrm{F}}(q_z)$. This might have been inferred from the result in eq 18 for circular slit approximation since, when

$$\eta \ll 1/\ln(q_{\mathrm{max}}/\Delta q_{\mathrm{res}}) \qquad (22)$$

the dependence of $R(q_z)$ on Δq_{res} vanishes; however, the numerical result suggests that the condition is not as strict as implied by eq 22.

The effect of finite resolution for $\eta > 1$ is illustrated explicitly by comparing the solid black line (—) in Figure 4, which corresponds to a slit ($h \times w$) = 1 mm × 3 mm, with the broken line (— — —), ($h \times w$) = 1 mm × 300 mm. Although the effect of the coarser transverse resolution leads to a significantly enhanced signal, the effect is considerably less than the divergence predicted by the infinitely wide slit. The horizontal resolution of 300 mm is also not physically realistic.

The real practical complication in measuring the reflectivity from liquid surfaces is to extract a quantitative result for $\Phi(q_z)$ from the measured reflectivity, Although one can, in principle, divide the measured $R(q_z)$ by the theoretically calculated integral of the capillary scattering, there is the unavoidable experimental problem of distinguishing between the signal that is reflected from the surface and diffuse scattering from a variety of other

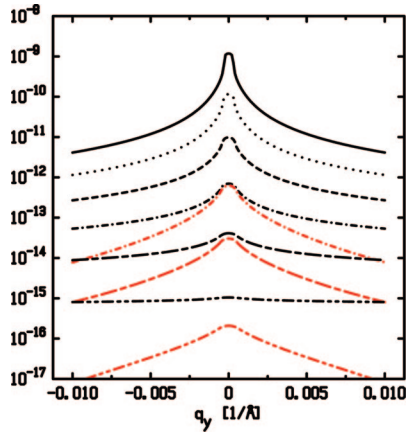

Figure 5. Integrals of the $1/q_{xy}^{2-\eta}$ form of $d\sigma/d^2\vec{q}_{xy}$ over a slit that is ($h \times w$) = (1 mm × 0.3 mm) and 600 mm from the sample. The black lines illustrate $I(\alpha;\beta,0)$, and the red lines indicate background-subtracted values $I(\alpha;\beta,0) - I(\alpha;\beta,0.03°)$. From top to bottom, the value of η = 0.46, 0.67, 0.90, 1.18, 1.49, and 1.91.

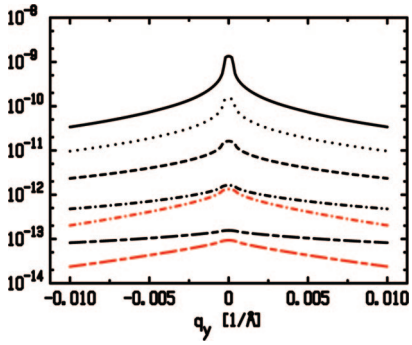

Figure 6. Integrals of the $1/q_{xy}^{2-\eta}$ form of $d\sigma/d^2\vec{q}_{xy}$ over a slit that is 10 times wider than the slit used for Figure 5, ($h \times w$) = (1 mm × 3.0 mm) and 600 mm from the sample. The black lines illustrate $I(\alpha;\beta,0)$, and the red lines indicate background-subtracted values $I(\alpha;\beta,0) - I(\alpha;\beta,0.3°)$. From top to bottom, η = 0.46, 0.67, 0.90, 1.18, and 1.49.

sources. These other sources could include small angle scattering from the atmosphere above the liquid surface (i.e., air scattering), diffuse scattering from any windows of the chamber surrounding the liquid, and diffuse scattering from the liquid below the surface. In almost all practical cases, diffuse scattering from the bulk liquid below the surface, as well as the background diffuse scattering from other sources, are generally slowly varying functions of $\vec{q}_{xy}$. For systems such as solids for which the specular signal is described by the $\delta(\vec{q}_{xy})$, the distinction can be achieved relatively easily by simply measuring the background scattering when $\beta \neq \alpha$ or $\theta \neq 0$, that is, $q_y = (2\pi/\lambda)[\cos\alpha - \cos\beta] \approx (2\pi/\lambda)\alpha(\beta - \alpha)$ or $q_x \approx (2\pi/\lambda)(\cos\beta)\theta$, and subtracting it from the scattering with $\beta = \alpha$ and $\theta = 0$, that is, $q_y = 0$. In principal, the same can be done for scattering from a liquid surface; however, in view of the $1/q_{xy}^{2-\eta}$ form, the subtraction is not so straightforward.

The black lines in Figure 5 illustrate calculations of $I(\alpha;\beta,0)/I_0$ from the surface of water with angles α = 5, 6, 7, 8, 9, and 10.2° and λ = 1.54Å. For these values, the lines correspond to (q_z,η) = [(0.71, 0.46), (0.85, 0.67), (0.99, 0.91), (1.13, 1.18), (1.28, 1.49), and (1.45, 1.91)]. The fact that the curve for η = 1.91 is nearly flat is a precursor to the fact that for $\eta > 2$ the intensity at the specular condition is actually smaller than that when $|\alpha - \beta| \neq 0$. To emphasize the subtle distinction between the δ-function in eq 11 and the capillary-induced cusp in eq 14, the calculations were done for a relatively narrow horizontal detector slit ($h \times w$) = (1 mm × 0.3 mm). As α increases, Δq_y increases proportionally and the central peak broadens; however, the more striking behavior is that as η approaches 2 the peak becomes less and less well-defined and would become increasing difficult to measure as η approaches 2. In particular, note that this calculation does not include nonsurface background scattering that would be present in nearly all real experiments. Thus, for example, although for this calculation the ratio of the intensity at the tail position of $q_y = -0.01$ Å^{-1} to the peak is ~0.044 for $\alpha = 8°$ ($\eta \approx 1.18$), when nonsurface sources of diffuse scattering are present the actual value could be considerably smaller. On the other hand, the fact that the $q_{xy} = 0$ cusp from surface diffuse scattering can be observed when $\alpha = 8°$ is illustrated by the red curves that display the calculated difference between the integral when the detector is in the plane of incidence, $\theta = 0$, and when it is shifted by the horizontal resolution, θ = (0.3 mm/600 mm)(180°/π) ≈ 0.03°,

$$\Delta I(\alpha;\beta,0.03°) = I(\alpha;\beta,0) - I(\alpha;\beta,0.03°) \qquad (23)$$

For example, at $\alpha = 8°$, the calculated ratio of the peak intensity, $\Delta I(8°;8°,0.03°)$ to the diffuse intensity in the tail when $\alpha - \beta \approx 1°$, corresponding to $q_{xy} = 0.01$ Å, is $\Delta I(8°;8°,0.03°)/\Delta I(8°;8.1°,0.03°) > 2500$, or nearly 2 orders of magnitude larger than the result when the $\theta = 0.03°$ is not subtracted. Assuming that the intensity of the nonsurface, or background diffuse scattering, at $\theta \approx 0.03°$ is equal to that at $\theta = 0$, these red curves should correspond to the empirically determined difference between the surface signals that are measured at $\theta = 0$ and 0.03°.

The implication of the above is to suggest that in the range of $1 < \eta \leq 2$ the surface structure factor $|\Phi(q_z)|^2$ can generally only be determined by measuring the difference

$$M(q_z) \equiv I(\alpha;\alpha,0) - \frac{1}{2}[I(\alpha;\alpha,+\Delta\theta) + I(\alpha;\alpha,-\Delta\theta)] \qquad (24)$$

The choice of $(1/2)[I(\alpha;\alpha,+\Delta\theta) + I(\alpha;\alpha,-\Delta\theta)]$ for the background, rather than just $I(\alpha;\alpha,\pm\Delta\theta)$ is simply to ensure against any unanticipated empirical $\pm\theta$ asymmetry. In any event, with the background subtracted away the value of $|\Phi(q_z)|^2$ can be obtained by dividing $M(q_z)$ by the numerically integrated value of the capillary prediction for the difference when $|\Phi(q_z)| = 1$.

The relatively small width of 0.3 mm for the horizontal detector slit in the previous example was chosen to emphasize the visibility of the singular cusp at $q_{xy} = 0$. In practice, the horizontal width can not be smaller than the width of the incident beam. The unfortunate fact is that the choice of a narrow incident beam generally requires some sacrifice in intensity. Furthermore, the horizontal angular resolution of 0.03° ≈ 0.5 mrad is close to what is often the practical resolution arising from either beam divergence or sample curvature. To avoid both the intensity loss and the complication associated with measuring the details of the shape of the incident beam, measurements are usually carried out with a somewhat larger horizontal width. The effect of the increased horizontal resolution can be seen by comparing the reduced visibility of the $q_{xy} = 0$ cusps for the calculations displayed in Figure 6, which were done with a 3.0 mm wide horizontal slit with the curves in Figure 5, for which the horizontal slit was only 0.3 mm. The cusp that remained visible up to values of η approaching 2 for the higher

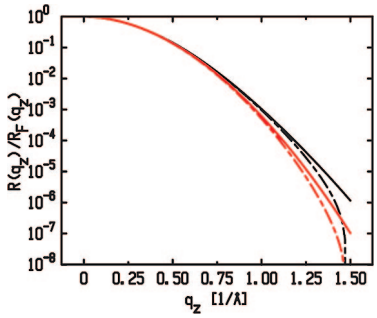

Figure 7. Calculated values of integrals of the $1/q_{xy}^{2-\eta}$ form of $d\sigma/d^2\vec{q}_{xy}$ for water using a detector slitd $(h \times w) = (1\text{ mm} \times 3.0\text{ mm})$(black) and (1 mm × 0.3 mm)(red) and 600 mm from the sample. The solid line corresponds to the integral at the specular condition, $\beta = \alpha$ and $\theta = 0$, and the broken line is the background-subtracted result.

resolution (Figure 5) have nearly disappeared by $\eta \approx 1$ for the coarser resolution curves in Figure 6.

The calculated effect on $R(q_z)/R_F(q_z)$ with background subtraction for water is illustrated in Figure 7 for two sets of slits $(h \times w) = (1\text{ mm} \times 3\text{ mm})$ with black lines and (1 mm × 0.3 mm) with red lines that more-or-less span typical reflectivity measurements. The solid lines indicate calculated integrals over the central portions of diffuse scattering profiles like those shown in Figure 5 when background is not subtracted. The broken lines illustrate the calculation with background subtractions corresponding to eq 24. The backgrounds are subtracted at 0.3° for the 3 mm wide slits and at 0.03° for the 0.3 mm wide slits. As can be seen for $q_z \leq 0.75$ the effects of both slit width and background subtraction are relatively negligible. This is essentially consistent with the diffuse line shapes that were illustrated above. For diffuse scattering at small values of q_z, the off-specular signal falls by roughly an order of magnitude relative to peak at relatively small values of q_y, and the primary contributions to the specular integration are achieved at correspondingly small values of q_y. On the other hand, as $q_z \rightarrow 1.45$ Å^{-1}, corresponding to $\alpha \approx 10.45$ or $\eta \approx 2$, the $1/q_{xy}^{2-\eta}$ form evolves from a peak at $\vec{q}_{xy} = 0$ to a minimum relative to larger $|\vec{q}_{xy}|$, and there should no longer be anything that can truly be identified as specular reflectivity. The broken lines, which corresponds to the background-subtracted signals do, in fact, vanish as $\eta \rightarrow 2$; however, the solid lines continue smoothly past $\eta = 2$. The point being made is that unless background subtraction is done there is no real way to ascertain whether or not the diffuse intensity described by the solid line originates in surface scattering. Furthermore, background subtraction is only viable so long as $\eta < 2$. Although the signals at larger values of q_z are generally greater for larger slits, so long as background subtraction is scaled along with the resolution, the effect of background subtraction is not terribly sensitive to the width of the slit.

As was mentioned above, the primary goal for all reflectivity measurements is to determine the surface stucture factor $\Phi(q_z)$. The solid points and the blue broken line in Figure 8 illustrate measurements and the calculated ratio of $R(q_z)/R_F(q_z)$ for the surface of liquid Sn as was measured by Shpykro et al.[30] The heavy black line illustrates the equivalent result after dividing the blue curve by the calculated thermal capillary effects. The published expression for $\Phi(q_z)$ and the corresponding density profile, $\rho_\infty^{-1}(d\langle\rho(z)\rangle/dz)$ are obtained by numerically fitting a model to the heavy black line. The red curve illustrates the ratio of $R(q_z)/R_F(q_z)$ that would have been obtained if the vertical slit was 1/10 of the value that was used in the experiment. In principle, the result of dividing the red curve by the calculated

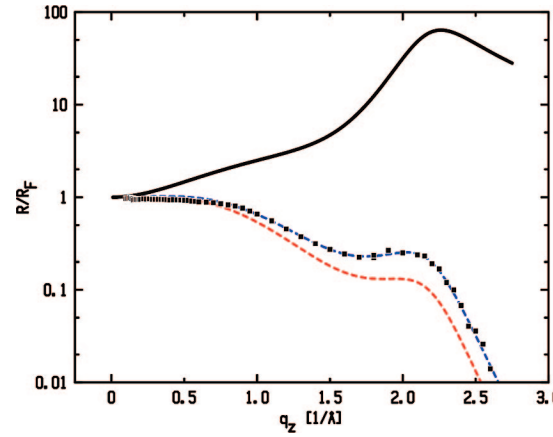

Figure 8. The dark points indicate measured values of $R(q_z)/R_F(q_z)$ for liquid Sn.[30] The broken blue line indicates a slight revision of the published fit to the Sn data. The broken red line indicates a simulated form for $R(q_z)/R_F(q_z)$ using a vertical slit that is a factor of 10 smaller than was used in the measurement. The heavy solid line indicates the result when either of these forms of $R(q_z)/R_F(q_z)$ is divided by the theoretical capillary integrals that are discussed in the text. For both cases the $\Delta\theta$ shift for the background subtraction was matched to the horizontal resolution.

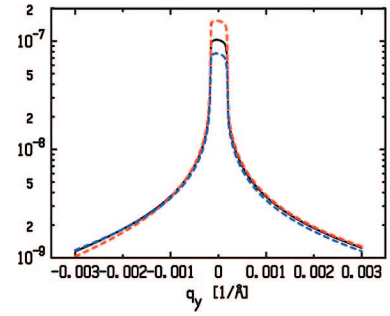

Figure 9. Calculated values of integrals of the $1/q_{xy}^{2-\eta}$ form of $d\sigma/d^2\vec{q}_{xy}$for water (solid black line) with a surface tension of 72 mN/m and models using 100 mN/m (red) and 60 mN/m (blue). The detector slits are $(h \times w) = (1\text{ mm} \times 3.0\text{ mm})$(black) and (1 mm × 0.3 mm)(red) and are 600 mm from the sample.

thermal capillary effects for this resolution would obtain the same heavy black line, and consequently the same $\Phi(q_z)$ and $\rho_\infty^{-1}(d\langle\rho(z)\rangle/dz)$. The point is that the correct final result is only obtained if the transformation from data to solid line is done using the same resolution function that was used in the measurement. Furthermore, the transformation depends on both the temperature and the surface tension of the liquid.

The final point that needs to be discussed is the practical determination of the value of η. In principal, the value of η can be determined by the shape of the tails of the curves of the diffuse intensity versus β, or q_z, as shown in Figures 5 and 6. On the other hand, a much more sensitive measure of the value of η is the ratio of the amplitude of the central peak to the amplitude of the tails. This is illustrated by the calculated curves in Figure 9. The solid black line illustrates the integral $I(\alpha = 3°;\beta,\theta = 0)$ of eq 12 for the water surface tension of 72 mN/m with detector slits of $(h \times w) = (1\text{ mm} \times 3.0\text{ mm})$(black) and (1 mm × 0.3 mm)(red) that are 600 mm from the sample. This corresponds to $q_z \approx 0.43$ Å^{-1} and $\eta \approx 0.16$. For these values, the $d\sigma/d^2\vec{q}_{xy} \sim q_{xy}^{-1.84}$. The red and blue curves were calculated with surface tensions of 100 mN/m for which $\eta \approx 0.12$ $(2 - \eta \approx 1.88)$ and 60 mN/m for which $\eta \approx 0.19$ $(2 - \eta \approx 1.81)$. Although the tails of all three curves are virtually identical, the peak heights are significantly different. Although the ratio of

the intensity of the central peak to that of the tails varies with the area of the resolution function, for any specific resolution the ratio is the most sensitive measure of η.

5. Summary

One objective of this article has been to demonstrate the basic difference between X-ray reflectivity from solid flat surfaces and from capillary roughened liquid surfaces. The principal point has been to illustrate the consequences of the fact that for a rigid flat surface the Fresnel reflection, corresponding to a differential cross section of the form $\delta^2(\vec{q}_{xy})$, is qualitatively different from the form for a liquid. Although gravitational effects cut off the $1/q_{xy}^{2-\eta}$ cusp at $\vec{q}_{xy} = 0$ before it can become a true singularity, the length scale at which this occurs is not usually resolvable by X-rays, and the angular dependence of the diffuse scattering can be treated as a singular cusp. When gravity is neglected there is no true specularly reflected signal. Nevertheless, scattering measurements similar to specular reflectivity that are made at small angles from liquid surfaces are virtually indistinguishable from those of solids. On the other hand, with increasing angles of incidence the $1/q_{xy}^{2-\eta}$ algebraic singularity becomes weaker (eventually vanishing when $\eta \geq 2$), and determination of the surface reflectivity requires thoughtful interpretation of the diffuse scattering.

Although most of the above illustrative calculations were done for water, when the results are viewed as a function of η they apply to virtually all liquids. For example, the surface tension of liquid gallium is about 10 times that of water implying that for gallium the $\eta = 2$ limit is only reached for $q_z \approx 4.5$ Å^{-1}. On the other hand, the surface tension at the interface between a hydrocarbon and fluorocarbon can be an order of magnitude less than that of water, implying that the $\eta = 2$ condition limits the specular reflectivity of ≤ 0.45 Å^{-1}.[31] Although the idealized criteria for optimizing measurement of the $1/q_{xy}^{2-\eta}$ singularity is to use the highest possible resolution (i.e., the smallest possible values of $\{\Delta q_x, \Delta q_y\}$), this ideal requirement must be balanced against both the cost of higher resolution in reducing the intensity and the complication in accounting for the shape of the incident beam.

The paper also addressed the issue of how the capillary roughness affects measurement of the structure factor for systems in which the structure factor $\Phi(q_z)$ defined in eq 6 is more complex than the simple Gaussian form of eqs 7 and 8. In some sense, the surface structure of nematic liquid crystals might be considered the prototypical example.[13,32] As these systems are cooled toward the smectic phase, the surface induces smectic order parallel to the surface with a layer spacing d_{layer}. The resultant X-ray reflectivity exhibits a temperature-dependent interference peak at $q_z = 2\pi/d_{\text{layer}}$. In principal, the amplitude of this interference peak should be reduced by the same capillary fluctuations as govern the reflectivity from water that was illustrated above. On the other hand, the smectic layering has an intrinsic temperature dependence, and there have not been any studies that attempted to separate the capillary effect from the intrinsic. Given this situation, the surface structure of liquid metals are better examples. As explained by Rice,[33] the electronic properties of the liquid metal induce atomic layering that is similar to the liquid crystal surface order, except the metal surface induced order does not exhibit an intrinsic temperature dependence. On the other hand, as was first shown for liquid gallium, the measured reflectivities have a significant capillary induced temperature dependence that must be taken into account in order to extract the intrinsic structure from the reflectivity.[25,30,34−43] The procedure for doing this was discussed in relation to eq 14.

Finally, it is shown that the most sensitive measure of the value of η, and thus of the surface tension, is the ratio of the intensity at the specular condition to that of the intensity of the tails of the diffuse scattering. An accurate measure of η requires accurate integrations of the scattering over the experimental resolution.

Acknowledgment. This work benefited from extensive collaborations that took place over a number of years. The list of these is relatively long and is adequately documented by the coauthor listing on the cited references. On the other hand, discussions with Ben Ocko, Masa Fukuto, and Oleg Shpyrko went beyond this and they warrant special thanks. This work was supported by the U.S. Department of Energy DOE Grant No. DE-FG02−88-ER45379.

Note Added after ASAP Publication. This paper was published ASAP on November 11, 2008. Figures 5 and 6 were changed. The revised paper was reposted on January 13, 2009.

References and Notes

(1) Daillant, J.; Gibaud, A., *X-ray and Neutron Reflectivity: Principles and Applications*; Springer: Berlin, New York, 1999.
(2) Roentgen, W. C. On a New Kind of Ray, A Preliminary Communciation, 1896, http://www.emory.edu/X-RAYS/century_05.htm.
(3) Compton, A. H. *Philos. Mag.* **1923**, *45*, 1121.
(4) Stauss, H. E. *Phys. Rev.* **1929**, *34*, 1021.
(5) Stauss, H. E. *Phys. Rev.* **1928**, *31*, 0491.
(6) Kiessig, H. *Annalen Der Physik* **1931**, *10*, 715.
(7) Kiessig, H. *Annalen der Physik* **1931**, *10*, 769.
(8) Kiessig, H. *Naturwissenschaften* **1930**, *18*, 847.
(9) Dershem, E. *Phys. Rev.* **1929**, *34*, 1015.
(10) Als-Nielsen, J.; McMorrow, D., *Elements of Modern X-ray Physics*; J. Wiley: New York, 2000.
(11) Parratt, L. G. *Phys. Rev.* **1954**, *95*, 359.
(12) Tolan, M., *X-ray Scattering from Soft-Matter Thin Films: Materials Science and Basic Research*; Springer-Verlag: New York, 1999.
(13) Pershan, P. S.; Als-Nielsen, J. *Phys. Rev. Lett.* **1984**, *52*, 759.
(14) Braslau, A.; Pershan, P.; Swislow, G.; Ocko, B.; Als, N. J. *Phys. Rev. A* **1988**, *38*, 2457.
(15) Ocko, B.; Wu, X.; Sirota, E.; Sinha, S.; Deutsch, M. *Phys. Rev. Lett.* **1994**, *72*, 242.
(16) Rice, S. A. *Nature* **1985**, *316*, 108.
(17) Pershan, P. S.; Balagurusamy, V. S. K.; Stoltz, S.; Shpyrko, O. G.; Meron, M.; Lin, B.; Deutsch, M. To be submitted for publication.
(18) Regan, M. J.; Kawamoto, E. H.; Lee, S.; Pershan, P. S.; Maskil, N.; Deutsch, M.; Magnussen, O. M.; Ocko, B. M.; Berman, L. E. *Phys. Rev. Lett.* **1995**, *75*, 2498.
(19) Regan, M. J.; Pershan, P. S.; Magnussen, O. M.; Ocko, B. M.; Deutsch, M.; Berman, L. E. *Phys. Rev. B* **1997**, *55*, 15874.
(20) Pershan, P. S. *Colloids Surfaces A* **2000**, *171*, 149.
(21) Batchelor, G. K., *An Introduction to Fluid Dynamics*; Cambridge University Press: Cambridge, U.K.; New York, NY, 2001.
(22) Buff, F. P.; Lovett, R. A.; Stillinger, F. H., Jr. *Phys. Rev. Lett.* **1965**, *15*, 621.
(23) Lovett, R.; Mou, C. Y.; Buff, F. P. *J. Chem. Phys.* **1976**, *65*, 570.
(24) Sinha, S. K.; Sirota, E. B.; Garoff, S.; Stanley, H. B. *Phys. Rev. B* **1988**, *38*, 2297.
(25) Tostmann, H.; DiMasi, E.; Pershan, P. S.; Ocko, B. M.; Shpyrko, O. G.; Deutsch, M. *Phys. Rev. B* **1999**, *59*, 783.
(26) Ashcroft, N. W.; Mermin, N. D. *Solid State Physics*; Holt, Rinehart, and Winston: New York, 1976.
(27) Braslau, A.; Deutsch, M.; Pershan, P. S.; Weiss, A. H.; Als-Nielsen, J.; Bohr, J. *Phys. Rev. Lett.* **1985**, *54*, 114.
(28) Schwartz, D. K.; Schlossman, M. L.; Kawamoto, E. H.; Kellogg, G. J.; Pershan, P. S.; Ocko, B. M. *Phys. Rev. A* **1990**, *41*, 5687.
(29) Daillant, J.; Bosio, L.; Benattar, J.; Meunier, J. *Europhysics-Lett.* **1989**, *8*, 453.
(30) Shpyrko, O. G.; Grigoriev, A.; Steimer, C.; Pershan, P. S.; Lin, B.; Meron, M.; Graber, T.; Gerbhardt, J.; Ocko, B. M.; Deutsch, M. *Phys. Rev. B* **2004**, *70*, 224206.
(31) Fukuto, M.; Gang, O.; Alvine, K. J.; Pershan, P. S. *Phys. Rev. E* **2006**, *74*, 031607.
(32) Als-Nielsen, J.; Christensen, F.; Pershan, P. S. *Phys. Rev. Lett.* **1982**, *48*, 1107.
(33) Rice, S. A. *Proc. Natl. Acad. Sci. USA* **1987**, *84*, 4709.

(34) Regan, M.; Pershan, P.; Magnussen, O.; Ocko, B.; Deutsch, M.; Berman, L. *Phys. Rev. B* **1996**, *54*, 9730.

(35) Regan, M.; Tostmann, H.; Pershan, P.; Magnussen, O.; DiMasi, E.; Ocko, B.; Deutsch, M. *Phys. Rev. B* **1997**, *55*, 10786.

(36) Balagurusamy, V. S. K.; Streitel, R.; Shpyrko, O. G.; Pershan, P. S.; Meron, M.; Lin, B. *Phys. Rev. B* **2007**, *75*, 104209.

(37) Shpyrko, O. G.; Huber, P.; Pershan, P. S.; Ocko, B. M.; Tostmann, H.; Grigoriev, A.; Deutsch, M. *Phys. Rev. B* **2003**, *67*, 115405.

(38) Huber, P.; Shpyrko, O.; Pershan, P. S.; Ocko, B. M.; Tostmann, H.; DiMasi, E.; Deutsch, M. *Phys. Rev. Lett.* **2002**, *89*, 035502.

(39) DiMasi, E.; Tostmann, H.; Ocko, B. M.; Pershan, P. S.; Deutsch, M. *Phys. Rev. B* **1998**, *58*, 13419.

(40) DiMasi, E.; Tostmann, H.; Ocko, B. M.; Pershan, P. S.; Deutsch, M. *J. Phys. Chem. B* **1999**, *103*, 9952.

(41) Tostmann, H.; DiMasi, E.; Pershan, P. S.; Ocko, B. M.; Shpyrko, O. G.; Deutsch, M. *Phys. Rev. B* **2000**, *61*, 7284.

(42) Tostmann, H.; DiMasi, E.; Shpyrko, O. G.; Pershan, P. S.; Ocko, B. M.; Deutsch, M. *Phys. Rev. Lett.* **2000**, *84*, 4385.

(43) Huber, P.; Shpyrko, O.; Pershan, P. S.; Ocko, B.; DiMasi, E.; Deutsch, M. *Phys. Rev. B* **2003**, *68*, 085401.

JP806113N